

## CAV2009 – Paper No. 43

### The partial cavity on a 2D foil revisited

**M. Hoekstra**

Maritime Research Institute Netherlands  
Wageningen, The Netherlands

**G. Vaz**

Maritime Research Institute Netherlands  
Wageningen, The Netherlands

#### ABSTRACT

The partial cavity on a 2D NACA0015 foil at 6 degrees angle-of-attack is studied numerically. Assuming the fluid to be a continuum of variable density, we solve the RANS equations, complemented with turbulence and cavitation models. Some important details of the mathematical model are pointed out first. We study then carefully what occurs in the numerical simulations in and near the cavity from the inception phase to the stage well before serious unsteadiness (cavity shedding) starts. By making the computations on grids of different densities we get an impression of numerical uncertainties. This is important for the interpretation and the subsequent comparison with what experimental investigations have learned us about the physics of these almost steady partial cavities on foils. The results show that close to inception a cavity exists while the boundary layer is non-separating. The liquid-vapour interface turns out not to be a material surface, neither at the front end nor at the tail of the cavity. It also appears that the widely accepted re-entrant jet model as conceived from free-streamline theory is not a good description of the flow at the tail. The confrontation of the numerical results with information from experiments indicates that there is agreement and corroboration in several respects, but also intriguing discrepancies are found which require further elucidation.

#### INTRODUCTION

The partial cavity on a 2D foil has been studied extensively in the past, both experimentally and numerically. Thus the knowledge and understanding of the observed phenomena have accumulated during the years. The occurrence and the shape of a partial cavity is not only dependent – as expected – on the foil shape, its orientation with respect to the incoming flow, the speed of that flow and the pressure level, but also – less expected – on the fluid viscosity and the fluid “quality”

(notably the content and the size spectrum of nuclei) as well as the foil surface properties. A wealth of information on the findings of many years of research and references to important papers on the subject can be found in Franc & Michel’s book about the fundamentals of cavitation [1]. They describe for example that various experimentalists have successively confirmed the strong relation between the appearance of cavitation and the behaviour of the boundary layer on the foil. Yet, there are unresolved issues left. Why is the pressure at the stagnation point aft of the partial cavity so low? Is the liquid just ahead of the cavity under tension (meta-stable state)? To what extent is the cavity surface a material surface? Is an attached partial cavity necessarily associated with flow detachment?

We have approached the problem from the numerical side. This comes with an obligation to consider carefully to what extent the outcome could be affected by modeling and discretisation errors; on the other hand, the amount of detail that we get in velocity, pressure and other variables is practically unachievable in an experiment. As in so many other applications, numerical studies can complement experiments to come to a full understanding of what is going on.

We have computed the flow past a NACA0015 foil at 6 degrees angle-of-attack. Under *wetted flow* conditions the RANS equations are solved, assuming incompressibility of the fluid. For *cavitating flow* simulations we adopt the concept of a continuum mixture fluid with variable density and viscosity. Again the RANS equations are solved for this mixture fluid, with an added transport equation for the vapour fraction, governing the evaporation and condensation processes. With this numerical model we have studied the flow details in and near a partial cavity, between the inception phase and the stage where shedding of vapour clouds starts, i.e. in the more or less stable regime for which we think the RANS model to be an

appropriate choice. Results have been obtained on three geometrically similar grids of varying density, giving a rough idea of uncertainties due to discretisation errors, which can be taken into account in the interpretation of the data.

In what follows, first a description of the mathematical model and its numerical treatment is given. In particular the special features of the equations, if applied to a variable-density continuum mixture fluid instead of a uniform-density incompressible fluid, are addressed. Then flow conditions for the foil are specified and the results of the numerical simulations are presented. Only afterwards the numerical results will be confronted with experimental information and a discussion of possible and impossible flow configurations ensues. Conclusions are drawn at the end of the paper.

## MATHEMATICAL MODEL

The numerical model for the simulation of the flow with and without cavitation refers to the RANS equations, supplemented with a transport equation for the vapour fraction and a turbulence model. We solve the equations in steady as well as unsteady mode, but only under conditions which result in steady or weakly unsteady flow, to avoid running into philosophical discussions about the meaning of unsteady RANS.

Below we shall present the primary equations to be solved. We shall then refer to a fundamental relation for the rate of change of some quantity  $\Phi$  contained in a material volume  $V$  moving in a velocity field  $\bar{u}$  which reads (see e.g. Chapter 3 of [2]):

$$\frac{d}{dt} \int \Phi dV = \int \left( \frac{\partial \Phi}{\partial t} + \nabla \cdot \Phi \bar{u} \right) dV = \int \left( \frac{D\Phi}{Dt} + \Phi \nabla \cdot \bar{u} \right) dV. \quad (1)$$

### Mass conservation

If in Eq. (1)  $\Phi$  is replaced by the mass density of the fluid, denoted by  $\rho$ , mass conservation is expressed by the equation

$$\frac{\partial \rho}{\partial t} + \nabla \cdot \rho \bar{u} = \frac{\partial \rho}{\partial t} + \bar{u} \cdot \nabla \rho + \rho \nabla \cdot \bar{u} = \frac{D\rho}{Dt} + \rho \nabla \cdot \bar{u} = 0. \quad (2)$$

We have omitted here the integral signs because Eq. (1) must hold for any material volume. For an incompressible fluid the density  $\rho$  is uniform and not changing in time, so that the equation reduces to the well-known condition:

$$\nabla \cdot \bar{u} = 0.$$

Ignoring the presence of non-condensable gas, the density of a mixture of the two phases liquid and vapour with volume fractions  $\alpha_l$  and  $\alpha_v$  respectively is:

$$\rho = \alpha_l \rho_l + \alpha_v \rho_v, \quad \alpha_l + \alpha_v = 1,$$

where  $\rho_l$  and  $\rho_v$ , the densities of liquid and vapour, may be temperature-dependent but are assumed not to vary in space or time. Substitution in Eq. (2) yields then either

$$\frac{\partial \alpha_v}{\partial t} + \nabla \cdot \alpha_v \bar{u} = \frac{S}{\rho_v}, \quad (3)$$

or

$$\frac{\partial \alpha_l}{\partial t} + \nabla \cdot \alpha_l \bar{u} = -\frac{S}{\rho_l}, \quad (4)$$

in which  $S$  is a source term given by

$$S = \frac{\rho_v \rho_l}{\rho_l - \rho_v} \nabla \cdot \bar{u},$$

implying

$$\nabla \cdot \bar{u} = -\frac{1}{\rho} \frac{D\rho}{Dt} = \frac{\rho_l - \rho_v}{\rho_l \rho_v} S = \left( \frac{1}{\rho_v} - \frac{1}{\rho_l} \right) S.$$

So  $S$  is directly proportional to the expansion rate of the fluid and a model for  $S$ , to be given below, governs the evaporation and condensation processes which create or destroy cavitation. Sometimes such models for  $S$  are called *mass transfer models*, which might be misleading, because it seems to suggest that the source term affects the mass conservation only, while, as we shall see, it plays a role in the momentum transfer as well as in the vorticity dynamics (as a matter of fact in any conservation equation, see Eq. (1)).

### Momentum conservation

The role of the source term in the momentum equation is twofold. First, by considering Eq. (1) with  $\rho \bar{u}$  replacing  $\Phi$ , we can write the momentum equation as

$$\frac{\partial \rho \bar{u}}{\partial t} + \nabla \cdot \rho \bar{u} \bar{u} = \bar{F},$$

where  $\bar{F}$  represents the sum of the pressure and viscous forces and possibly external forces. The equation can be rewritten as

$$\frac{D\rho \bar{u}}{Dt} = \bar{F} - \rho \bar{u} \left( \frac{1}{\rho_v} - \frac{1}{\rho_l} \right) S = \bar{F} - \bar{u} \frac{D\rho}{Dt},$$

which implies the alternative formulation

$$\frac{D\bar{u}}{Dt} = \frac{\bar{F}}{\rho}.$$

This clearly brings out that the same force (with the pressure gradient as the most relevant contribution) will cause a stronger acceleration (or deceleration, if the force is negative) of the mixture fluid with decreasing density. Or conversely, if such strong accelerations are not observed the force must have adjusted.

The second effect of the source term on the momentum transfer is via the stress tensor. The dynamic viscosity is, like the density, expressed as

$$\mu = \alpha_l \mu_l + \alpha_v \mu_v.$$

But next to that, the stress tensor used in the Navier-Stokes equations contains also the expansion rate:

$$T_{ij} = -p \delta_{ij} + 2\mu \left( e_{ij} - \frac{1}{3} e_{ii} \delta_{ij} \right),$$

with

$$e_{ij} = \frac{1}{2} \left( \frac{\partial u_i}{\partial x_j} + \frac{\partial u_j}{\partial x_i} \right),$$

implying

$$e_{ii} = \frac{\partial u_i}{\partial x_i} = \nabla \cdot \bar{u}.$$

If the RANS equations are applied to a mixture fluid, this term should of course be included.

## Vorticity dynamics

Cavitation observations often reveal complicated vortex structures and it is worthwhile to check also what the assumption of a variable-density mixture fluid implies for the equation governing the vorticity dynamics. This equation, following from applying the curl operator to the momentum equation, reads

$$\frac{D\bar{\omega}}{Dt} = \bar{\omega} \cdot \nabla \bar{u} - \bar{\omega} \nabla \cdot \bar{u} + \frac{1}{\rho^2} (\nabla \rho \times \nabla p) + \frac{\nabla \times \bar{B}}{\rho} + VT.$$

in which  $VT$  is shorthand for the viscous terms, while  $\bar{B}$  is the body force per unit of volume.

The rate of change of the vorticity vector is thus influenced by five contributions. Two of them vanish if the fluid is incompressible, but are important in cavitation simulations, viz. the second and third term on the right-hand side. The third term, is the so-called "baroclinic torque" which is often mentioned to be active in the tail part of an attached sheet cavity. In contrast, the second term is hardly ever mentioned, while it must play a significant role. It involves the rate of expansion as well as the vorticity vector itself. So it is not a production term in the strict sense that it can create vorticity where there was no vorticity before. But it will enhance the vorticity where the expansion rate is negative, and reduce the vorticity in the opposite case. Upon collapse of a vapour bubble, all vorticity it contains will be focused in a much smaller volume. The high vorticity observed at the tail of a partial cavity is partly due to this term.

## Turbulence model

Needless to say that in the transport equations constituting the turbulence model the expansion rate plays its role as well. Like in the momentum equation, as long as the equations are formulated and solved in the strong conservation form, nothing needs to be added explicitly, but it is good to be aware of effects not present in an incompressible fluid.

In all computations presented in this paper the turbulence model, a necessary ingredient of RANS simulations, is the SST version of the  $k-\omega$  model [3]. This model, like most of its competitors, has been tuned to operate well in fully-developed turbulent boundary layers. But when computing the flow past a foil, one has to cope with the transition from a laminar to a turbulent flow state as well. For want of something better, we let the turbulence model, without adjustments, govern the transition process as well. To our experience, this gives fair results, but we realize that due consideration must be given to the uncertainty about the location of transition in interpreting them. (Similar considerations apply to experiments, by the way).

An as yet unresolved issue is whether turbulence models require specific modification for cavitating flows. Sometimes an extra reduction of the dynamic eddy viscosity is applied in the region where cavitation occurs. Such modifications have not been applied by us because their merit can only usefully be investigated with negligible discretisation errors, a task which we have not yet finished.

## Source term

In order to complete the mathematical model, the source term  $S$  (or, equivalently, the expansion rate), controlling

evaporation and condensation, must be set or expressed in terms of the other variables. Several formulations have been proposed, practically all having the deviation of the local pressure from the saturated vapour pressure,  $p-p_v$ , as well as the volume fraction ( $\alpha_v$  or  $\alpha_l$ ) itself as parameters. In this paper we follow largely Sauer's model [4], which with slight adjustments gives the following expressions for the source term:

$$\frac{S}{\rho_v} = (4\pi R^2 n_0) (1 - \alpha_v) \sqrt{\frac{2 |p_v - p|}{3 \rho_l}} \quad \text{for } p < p_v, \quad (5a)$$

$$\frac{S}{\rho_v} = -\frac{3\alpha_v}{R} \sqrt{\frac{2 |p_v - p|}{3 \rho_l}} \quad \text{for } p \geq p_v, \quad (5b)$$

in which the "bubble radius"  $R$  is related to  $\alpha_v$  and  $n_0$  by

$$\frac{4}{3} \pi R^3 n_0 = \frac{\alpha_v}{1 - \alpha_v},$$

and  $n_0$  is a free parameter, representing the number of nuclei per unit of volume. By eliminating  $R$  from Eqs. (5a) and (5b) it can be shown that the source term is anti-symmetric with respect to  $p=p_v$ , viz:

$$\frac{S}{\rho_v} = 3 \left( \frac{4}{3} \pi n_0 \right)^{1/3} (1 - \alpha_v)^{1/3} \alpha_v^{2/3} \text{sign}(p_v - p) \sqrt{\frac{2 |p_v - p|}{3 \rho_l}}.$$

but the expressions (5a) and (5b) are used in the numerical implementation. Among other things, it allows us to set a minimum ( $3 \times 10^{-5}$  m) and a maximum (1.0 m) for  $R$  to avoid anomalous behaviour for  $\alpha_v \rightarrow 0$ ,  $R \rightarrow 0$  and  $\alpha_v \rightarrow 1$ ,  $R \rightarrow \infty$ . The square root function of  $p-p_v$  in Eqs. (5a) and (5b) has its foundation in the Rayleigh-Plesset equation. The source term is plotted as a function of  $\alpha_v$  and  $(p-p_v)/\rho$  in Fig. 1.

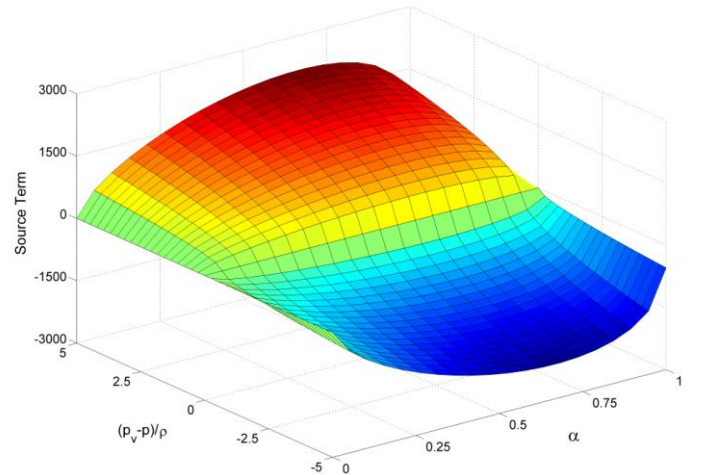


**Figure 1:** Sauer's source function

We notice that Sauer's model gives a scale-dependent source strength if the parameter  $n_0$  is considered as a fluid property. After non-dimensionalisation the source term becomes:

$$\frac{Sc}{\rho_v U_\infty} = -3 \left( \frac{4}{3} \pi n_0 c^3 \right)^{1/3} (1 - \alpha_v)^{1/3} \alpha_v^{2/3} \text{sign}(Cp + \sigma) \sqrt{\frac{1}{3} |Cp + \sigma|}.$$

It means that for the flow around two foils of different size but at the same cavitation number and Reynolds number the source term is weaker for the smaller foil. This is physically not unrealistic as explained in [5, section 5.4]. This effect can of course be suppressed by choosing  $n_0$  proportional to  $1/c^3$ .

For use in later discussions it is important to list here the main properties of the source term:

1. it is non-zero for  $0 < \alpha_v < 1$  only;
2. it is positive for  $p < p_v$  only;
3. it is negative for  $p > p_v$  only;
4. referring to Eq. (1) and Eq. (3), the following relation holds for any material volume  $V$ :

$$\frac{d}{dt} \int \alpha_v dV = \int \frac{S}{\rho_v} dV . \quad (6)$$

If the volume is chosen large enough to contain the complete cavity, it implies that the rate of change of the cavity volume equals the integrated source term. In a steady flow the integral of  $S$  must vanish. (It provides an excellent check on numerical accuracy, particularly for unsteady flow simulations).

5. in a steady flow and with  $\rho_l \gg \rho_v$  Eq. (3) can be approximated as

$$\frac{S}{\rho_v} \approx \frac{\bar{u} \cdot \nabla \alpha_v}{1 - \alpha_v} , \quad (7)$$

which shows that under such conditions the source term must vanish where the flow is aligned with the liquid-vapour interface ( $\bar{u} \cdot \nabla \alpha_v = 0$ ).

We like to emphasize that only the second and the third property are related to the chosen model for  $S$  (most currently available models share these properties, though, the model proposed by Kunz [6] being a noteworthy partial exception), the others hold for any model.

## NUMERICAL SOLUTION

The numerical solution of the six equations (two momentum components, mass conservation, vapour fraction equation and two equations of the turbulence model) is based on finite-volume discretisation with all variables collocated at cell centers. Although the equations are coupled, they are solved in a segregated way. By iteration the coupling is restored (SIMPLE algorithm). As is common in this approach a fourth derivative of the pressure is added as a regularization term to the continuity equation (pressure-weighted interpolation) to avoid checkerboarding.

Three iteration loops can be distinguished: the time loop to advance the solution in time (not applicable to steady mode); the outer loop to solve the coupled equation set in each time step; the inner loop, to solve each equation separately, accounting for non-linearity and deferred corrections.

The discretisation is nominally second order in space, except for the convection terms in the turbulence model equations and the transport equation for  $\alpha_v$  (first-order upwind). The QUICK scheme is applied to the convection terms of the momentum equations. So-called compressive (or anti-diffusive) schemes, meant to keep interfaces sharp, have not been applied.

All computations were started in steady mode. A truly steady state solution could thus be obtained for flows with small cavities. Upon lowering the cavitation number, the steady mode resulted in a limit cycle process; in those cases the computations were continued in unsteady mode. For the computations in unsteady mode an implicit second order backward discretisation scheme was used for the time derivatives.

Systems of algebraic equations are solved with GMRES, using an incomplete LU decomposition as preconditioner.

Some further information on our flow code can be found in [7, 8].

## NUMERICAL RESULTS

We simulate the 2D flow past the NACA0015 foil at 6 degrees angle-of-attack in a water tunnel. The foil shape is given by an analytical expression [9]. This expression implies a finite thickness at the tail, amounting to 3.15 per cent of the chord length. Instead of modifying the shape to get a pointed aft end, we have just rounded the trailing edge.

We have chosen a chord length of  $0.2 \text{ m}$  and a height of the tunnel test section equal to  $0.57 \text{ m}$ . A coordinate system has been adopted with the origin at the centre of gravity of the foil, i.e. at a relative chord position of 0.3086, at midheight of the tunnel. The foil has been rotated by 6 degrees about this origin. With the inlet at  $x = -0.46172 \text{ m}$  (two chords upstream of the leading edge) and the outlet at  $x = 0.93828 \text{ m}$  (four chords downstream of the trailing edge) we arrive at the configuration displayed in Fig. 2.

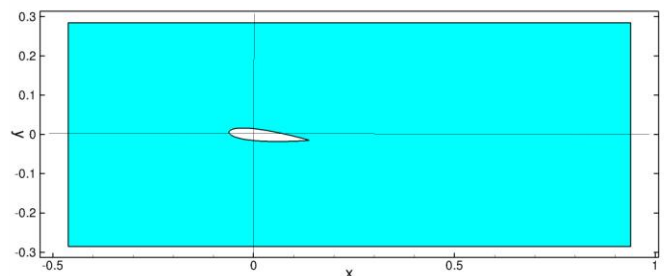
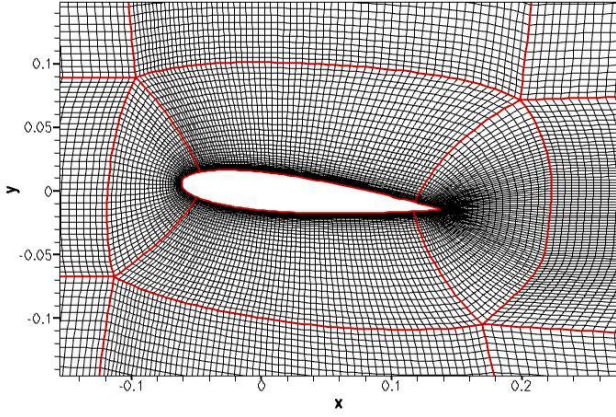


Figure 2: Domain size and foil position

Three grids of varying density were set up. In all cases a block-structured grid has been employed, consisting of an O-grid around the foil, embedded in an H-grid (12 blocks). Hexahedral cell shapes (quadrilaterals in 2D) have been used exclusively. An impression of the (coarsest) grid near the foil can be obtained from Fig. 3.

Full resolution of the near-wall flow is obtained by applying grid contraction towards the foil surface. The maximum height of wall-adjacent cells is non-dimensionally smaller than  $y_+ = 1$  in the wetted flow (no wall functions used). In refining the grids, care has been taken to make them geometrically similar so that a proper convergence study can be made. Grid G3 has twice as many cells in both coordinate directions as grid G1, i.e. grid G3 is obtained by splitting each cell of grid G1 into four sub-cells. Grid G2 has an intermediate density. The number of grid cells and the number of cell edges on the foil are summarized in Table 1.



**Figure 3:** Grid G1 in the vicinity of the foil

grid	# cells	cell size	# edges on foil
G1	27,808	2.0h	234
G2	62,568	1.5h	351
G3	111,323	1.0h	468

**Table 1:** Grid characteristics (h = “typical cell size”)

With a foil chord length of  $c=0.2$  m and an inflow velocity of  $U_\infty=6$  m/s, we arrive at a characteristic Reynolds number of  $Rn=1.2 \times 10^6$ . The liquid and vapour densities were set as  $\rho_l = 998.0$  kg/m<sup>3</sup> and  $\rho_v=0.024$  kg/m<sup>3</sup> (i.e. true physical values for a temperature of 24 °C). A low free-stream turbulence level was chosen, giving an eddy viscosity  $\mu_t=0.01\mu_i$ , where  $\mu_i$  is the dynamic viscosity of water ( $\mu_i=1.002 \times 10^{-3}$  kg/ms). The vapour dynamic viscosity was set at  $\mu_v=1.02 \times 10^{-5}$  kg/ms.

Boundary conditions were chosen as follows. On the foil surface zero velocity was imposed, while the pressure and vapour volume fraction were extrapolated from the interior solution. At the inlet plane a uniform speed  $u=U_\infty$  in the  $x$ -direction was imposed as well as a zero vapour volume fraction, while at the outlet a uniform pressure  $p=0$  was prescribed and a zero normal gradient for all other quantities. The outlet pressure was also used as the reference pressure  $p_\infty=p_{outlet}=0$ . On the top and bottom walls free-slip boundary conditions were applied. For the turbulent quantities the boundary conditions defined in [3] were used.

Calculations in unsteady mode were done with a time step of  $\Delta t=0.0005$  s, or non-dimensionally  $\Delta t U_\infty/c = 0.015$ . The free parameter of Sauer’s model, the number of nuclei per unit of volume, was fixed at  $n_0=10^8$  (100 nuclei per cm<sup>3</sup>).

### Wetted flow

The wetted flow was computed first to get the level and location of  $Cp_{min}$  and the lift and drag coefficients. The results are summarized in Tables 2 and 3. In Table 3 the pressure component of the lift coefficient and the frictional component of the drag coefficient have been given as well. The missing components  $CL_f$  and  $CD_p$  follow from  $CL-CL_p$  and from  $CD-CD_f$ , respectively.

grid	$Cp_{min}$	$Cp_{max}$	$y+_{min}$	$y+_{max}$
G1	-2.0832	1.0135	0.016	0.788
G2	-2.0796	1.0144	0.013	0.511
G3	-2.0803	1.0133	0.009	0.381

**Table 2:** Extrema for  $Cp$  and  $y+$  in wetted flow

grid	CL	CD	$CL_p$	$CD_f$
G1	0.66329	0.014323	0.66320	0.00859
G2	0.66605	0.014190	0.66597	0.00876
G3	0.66731	0.014178	0.66772	0.00882

**Table 3:** Lift and drag coefficients for wetted flow

That the  $Cp_{max}$  in Table 2 is slightly above 1.0 is because we simulate a tunnel configuration. There is a small pressure drop from inlet to outlet (a direct consequence of the momentum balance) and we have taken the pressure at outlet as the reference pressure for  $Cp$ .

The convergence of  $CL$  and  $CD$  with grid refinement is monotone. The estimated numerical uncertainty of the  $CL$ -value on the finest grid is below  $\pm 0.25$  per cent. The convergence of  $Cp_{min}$  and  $Cp_{max}$  is not monotone, but the variation in value is below 0.0040 for  $Cp_{min}$  and 0.0015 for  $Cp_{max}$ .

It is relevant to mention that the wetted flow did not show boundary layer separation. The boundary layer is laminar at the leading edge but becomes turbulent further downstream. Due to the difference in the pressure distribution on suction and pressure side, turbulence activity starts on the suction side at a relative chord position closer to the leading edge than on the pressure side, with little grid dependence. As an illustration, Fig. 4 shows two isolines of the eddy viscosity  $\mu_t=\mu$  and  $\mu_t=10\mu$  near the nose of the foil. It demonstrates that the flow at the leading edge is laminar and that transition takes place over quite some distance, since at  $\mu_t=10\mu$  the flow is not yet fully turbulent at the given Reynolds number (the maximum level of the non-dimensional eddy viscosity in this flow is above 300).

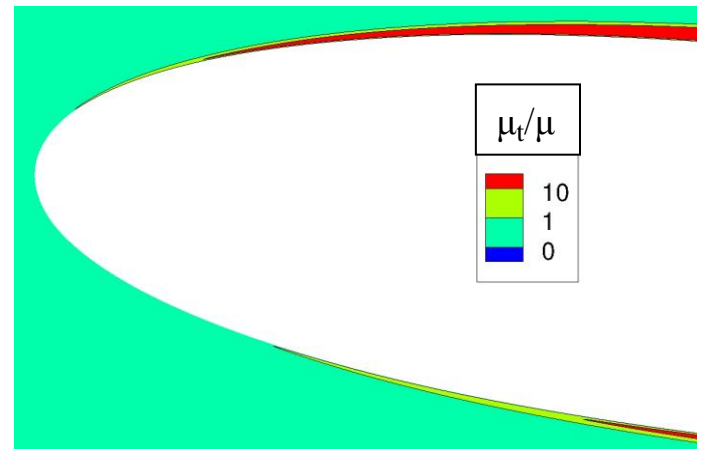


**Figure 4:** Eddy viscosity relative to molecular viscosity in wetted flow on grid G3

### Cavitating flow global results

The wetted flow results have  $C_{p\_min} \approx -2.08$ . Defining the cavitation number as

$$\sigma = \frac{P_\infty - P_v}{\frac{1}{2} \rho U_\infty^2},$$

inception occurs at  $\sigma = -C_{p\_min}$ . To study the development of the cavitation we computed the flow at  $\sigma=2.0$  and subsequently lowered the cavitation number in steps of 0.10 to  $\sigma=1.4$ . We start with giving the reader an impression of the global results, before embarking on a more detailed description of the flow behavior.

The variation of the lift and the drag with  $\sigma$  on grid G3 is given in Table 4; the table includes also the length of the cavity (measured on the  $\alpha_v=0.5$  contour line) relative to the chord length. The lift increases until a maximum is reached at  $\sigma=1.9$  ( $CL=0.6778$ ) and decreases then monotonically, leading to a loss in lift of some 8% at  $\sigma=1.4$ . An opposite trend is found for the drag: after an initial decrease, it increases with lower  $\sigma$ .

$\sigma$	CL	CD	CL/CD	$\ell/c$
>2.1	0.6673	0.0142	47.1	-
2.0	0.6728	0.0138	48.8	0.032
1.9	0.6778	0.0133	50.8	0.070
1.8	0.6755	0.0136	49.7	0.108
1.7	0.6657	0.0146	45.4	0.144
1.6	0.6524	0.0167	39.1	0.181
1.5	0.6366	0.0196	32.4	0.217
1.4	0.6179	0.0235	26.2	0.250

**Table 4:** Variation of lift, drag and cavity length with  $\sigma$  on grid G3

$\sigma$	$C_{p\_min}$	$-\sigma C_{p\_min}$	$S_{cav\_max}$	$S_{cav\_min}$
>2.1	-2.080	< 0	-	-
2.0	-2.079	0.079	38.5	-43.3
1.9	-2.031	0.131	49.5	-70.8
1.8	-1.950	0.150	53.2	-49.3
1.7	-1.856	0.156	54.1	-36.3
1.6	-1.758	0.158	54.5	-24.3
1.5	-1.655	0.155	53.9	-18.6
1.4	-1.552	0.152	53.4	-13.1

**Table 5:** Variation of  $C_{p\_min}$  and non-dimensional source term extremes with  $\sigma$  on grid G3

Table 5 gives information on the minimum pressure in the flow and on the extreme values of the non-dimensional source in the  $\alpha_v$ -equation:  $S_{cav} = Sc / (\rho_v U_\infty)$ . Interesting is that in all cavitating flow simulations the lowest pressure is below the vapour pressure. We will give further comments on this feature below. The maximum underpressure ( $-\sigma C_{p\_min}$ ), occurring at the front end of the cavity, tends to become more or less constant with decreasing  $\sigma$ . So while the cavity keeps growing, the difference between the minimum pressure and the vapour pressure as well as the maximum of the source term (both at the front end of the cavity) stabilize.

The development of the cavity with decreasing cavitation number is shown in Fig. 5. We have drawn the  $\alpha_v=0.5$  contour line as an outline of the cavity.

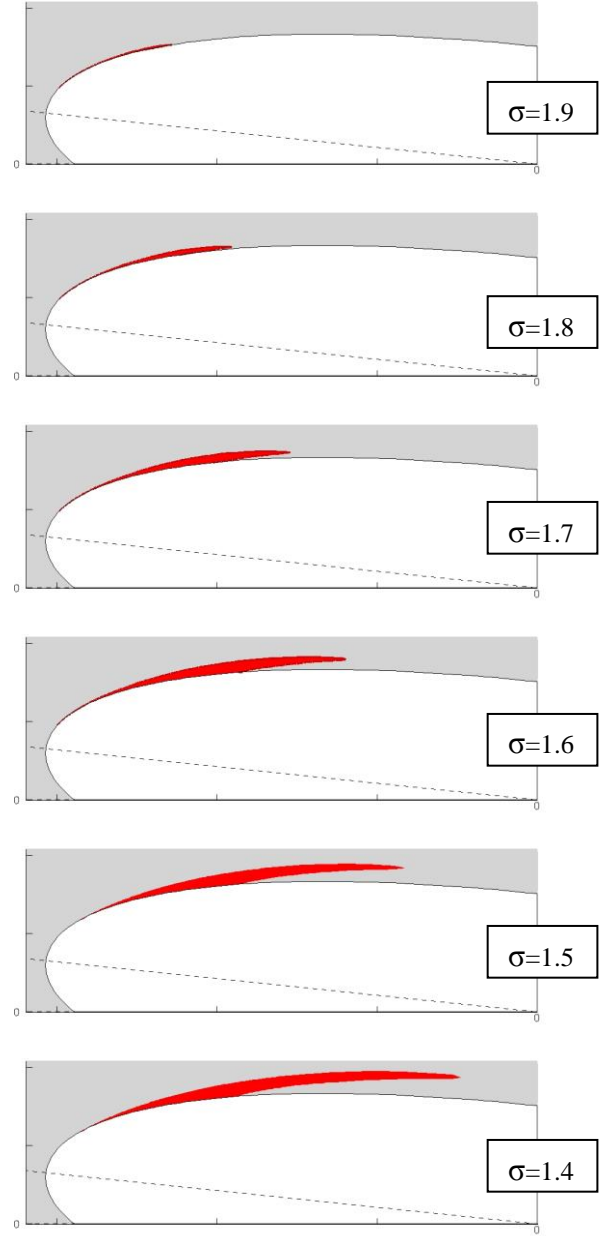


**Figure 5:** Computed cavity contour ( $\alpha_v=0.5$ ) for  $1.4 < \sigma < 1.9$  (dashed line is nose-tail line of the foil)

### Cavitating flow near inception ( $2.08 > \sigma > 1.9$ )

We proceed with describing the details of the flow behavior close to inception. The cavitation model adopted implies possibly weak but finite vapour production at any location where the pressure is below the vapour pressure,  $p < p_v$ ; the possibility of static or thermal delay is not included. Thus at  $\sigma=2.0$  some vapour is produced which appears as a very thin cavity. The length of the cavity  $\ell$  (measured on the  $\alpha_v=0.5$  contour line) is about 3.2 per cent of the chord and has a length/thickness ratio in the order of 400. There is not a plateau of uniform pressure in the cavity. The lowest pressure occurs at

the front end of the cavity. Because it is below  $p_v$ , the source term is positive there. Since the flow is steady, Eq. (6) implies that there must be compensating negative sources, which are found at the cavity tail. There is no flow reversal. Although the cavity can be viewed as an attached cavity in the sense that its position is locked with respect to the foil, the vapour is produced, then travels along the foil and finally condensates. Consequently, some streamlines must enter the cavity and leave it further downstream; the cavity surface cannot be a material surface. Although the cavity is very thin, it is noteworthy that it has the characteristic shape of a sheet cavity with liquid under its tail. In other words the tail of the cavity is lifted from the foil. Apparently the shape of the cavity is here a result of the velocity distribution (full condensation is accomplished over a longer distance for higher velocity) rather than of a re-entrant jet. Turbulence activity is delayed compared to the wetted flow and is seen only aft of the cavity.

At  $\sigma=1.9$  the cavity length has grown to 7.0 per cent of the chord. The length/thickness ratio has come down to 95. Though the cavity is thin, the interface between liquid and vapour is even thinner; part of the cavity is a 100 per cent vapour region. The flow underneath the cavity tail is on the verge of separation

### Features of the flow at $\sigma=1.8$

At  $\sigma=1.8$  a flow reversal zone has established itself under the tail of the cavity. Fig. 6 shows some details. Similar flow patterns in and near a partial cavity on other objects can be found in e.g. [6], [10] and [11]. At the front end of the cavity the streamlines penetrate the liquid-vapour interface, while they diverge strongly due to the expansion of the fluid, so that the angle between streamline and interface is small. Flow reversal sets in only where the cavity tail lifts from the foil surface. At this stage there is no vapour in the flow recirculation zone.

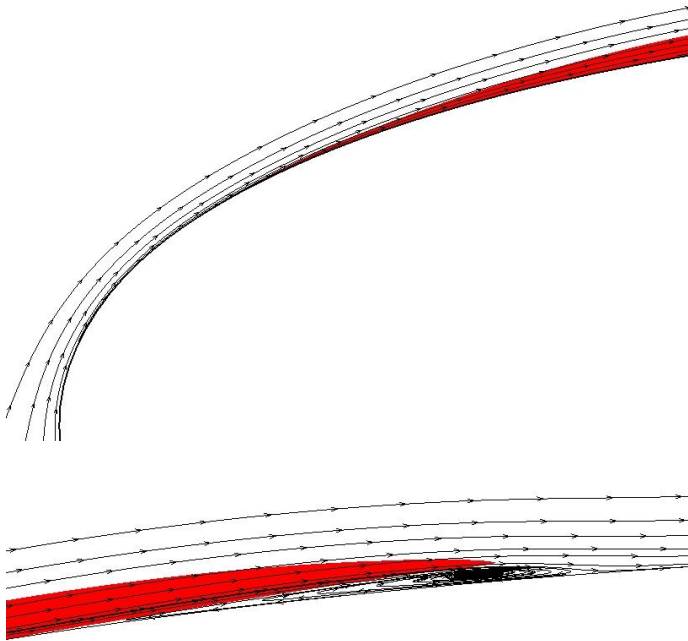


**Figure 6:** Streamlines and cavity contour ( $\alpha_v=0.5$ ) at front end (top) and aft end (bottom) at  $\sigma=1.8$  (grid G3)

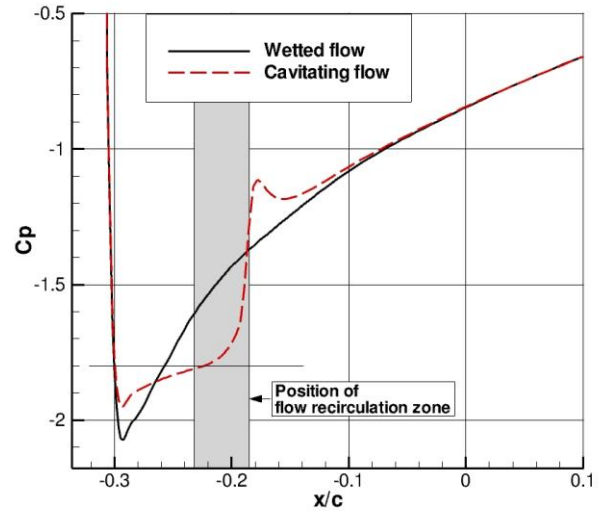


**Figure 7:** Comparison of pressure distribution on the nose of the foil at  $\sigma=1.8$  and in wetted flow (grid G3)

Informative and illuminating is the associated change of the pressure distribution on the suction side of the foil, illustrated in Fig. 7. A comparison is shown of the pressure distributions in the wetted flow and the cavitating flow ( $\sigma=1.8$ ), while the position of the recirculation zone is marked with a grey band. The level of the vapour pressure is indicated with a horizontal line at  $C_p=-1.8$ . The cavity extends from  $x/c=-0.299$  to  $x/c=-0.191$  ( $l/c=0.11$ ). The pressure on the foil in the cavitating flow is, compared to the wetted flow pressure, first higher, then lower and again higher. This corresponds of course with the global change in streamline curvature. In the wetted flow the convexity of the streamlines is slightly less than the convexity of the foil geometry due to the growth of the boundary layer. In the cavitating flow the convexity of the streamlines is, relative to the wetted flow, first reduced then increased and again reduced, in accordance with the expansion of the fluid as a result of cavity formation.

Evidently, the pressure becomes different from the pressure in wetted flow only after the cavity has grown somewhat. The minimum pressure is below the vapour pressure; and it must be so, because else the source term would vanish (property 2 of the source term) and the cavity would disappear. It must be said that the pressure distribution at the front end can easily be manipulated with the formulation used for the source term in the cavitation model. In Sauer's model the evaporation starts slowly because the "bubble radius"  $R$  is very small for small vapour fraction (see Eq. (5a)). By replacing  $R$  by a constant the evaporation starts impulsively which tends to make the source term bigger, but the pressure will react and rise to a level closer to the vapour pressure so that a new equilibrium is established without resulting in significant changes of the flow or the cavity. So there is a delicate interplay between source and pressure gradient.

### Flow in the developed cavity ( $\sigma=1.6$ )

Upon further lowering the cavitation number, not only the cavity grows (with a strong reduction of the length-thickness ratio), but also the recirculation zone, the flow detachment point now being inside the cavity and approaching gradually the front end of the cavity. Also a plateau in the pressure distribution at  $C_p=-\sigma$  appears. Moreover, the numerical solutions do not converge to steady state anymore. Slight fluctuations persist in the tail region of the cavity.

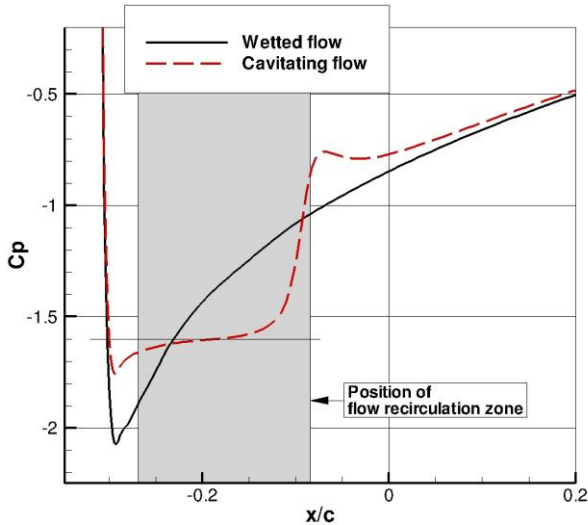


**Figure 8:** Comparison of pressure distribution on the nose of the foil at  $\sigma=1.60$  and in wetted flow (grid G2)

We shall now illustrate the main features of the developed cavity by presenting the details of the results at  $\sigma=1.60$ . First of all, Fig. 8 gives, in a similar style as Fig. 7, the change in the pressure distribution with respect to the wetted flow for  $\sigma=1.60$ . The length of the cavity is  $\ell/c=0.18$  (from  $x/c=-0.30$  to  $x/c=-0.12$ ) and the length-height ratio is about 20.

Fig. 9 shows the cavity at  $\sigma=1.60$ , computed on each of the three grids, by a display of the vapour fraction distribution. The liquid-vapour interface tends to get thinner with grid refinement where the flow is roughly aligned with the interface. Although the cavity length stays almost the same with grid refinement, it is clear that the cavity outline changes somewhat. In our calculations we found that the total vapour volume decreases with grid refinement for all cavitation numbers. It is an indication that numerical cavitation simulations have to be done on (locally) quite fine meshes to get rid of mesh resolution effects on the solution. These effects are in the first place apparent in the thickness of the interface and the penetration depth of liquid flow under the cavity. On the other hand, on all three grids the underlying flow pattern is essentially the same.

This underlying flow pattern is only slightly different from what we saw at  $\sigma=1.80$ . The recirculation zone is more developed and the flow reattachment point has moved aft due to the increased size of the cavity. As a result the flow detachment point, which has moved only slightly, is relative to the cavity much further upstream and in the vapour region. It means that the recirculation zone is now partly filled with vapour. Since the recirculation zone is a material volume, the

relation (6) must hold: in steady flow conditions the total source strength within the recirculation zone must vanish. In other words, the vapour created in the recirculation zone is also destroyed there. Thus the flow inside the zone is in a cyclic process of evaporation and condensation. As before, the cavity may be identified as an “attached” cavity, but in it the fluid, in vapour or in liquid phase, is continuously in motion.

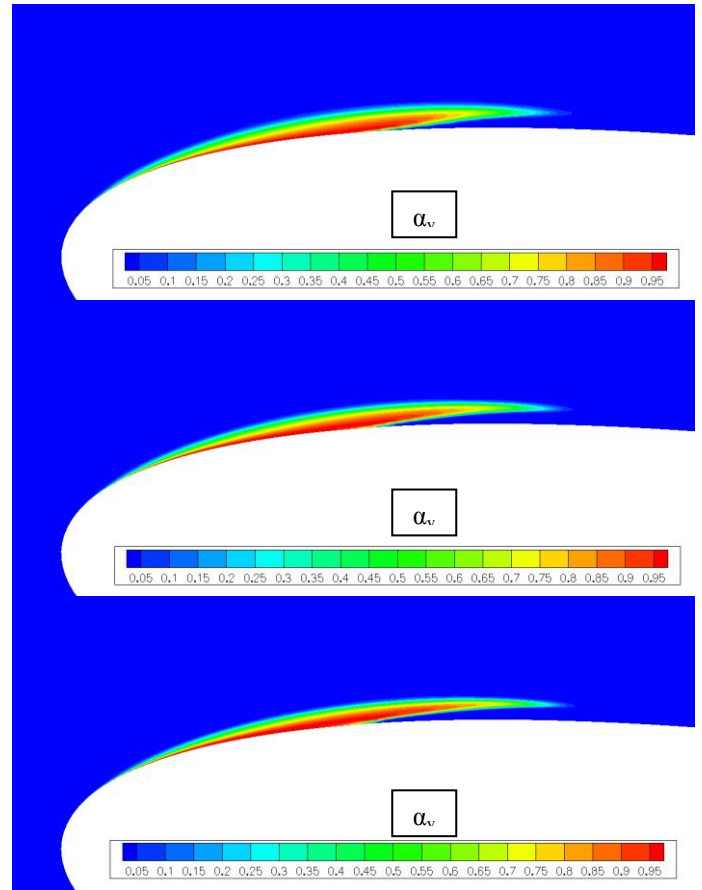


**Figure 9:** Vapour fraction distribution in cavity at  $\sigma=1.6$  on grid G1(top), G2(middle) and G3(bottom)

### Flow close to aft end of cavity

Turning next to the aft end of the cavity, we observe that the flow pattern, as it appears in our calculations, is in gross conflict with what earlier publications have made us believe. We have copied in Fig. 10 a sketch from [1]. It is a concept of the re-entrant jet flow structure from free-streamline theory. It has been around for more than 30 years and has been adopted in some potential-flow based methods for computation of cavitation. It is an ultimate attempt to let the cavity surface be a material surface. Although it is acknowledged by Franc & Michel to be a pattern that cannot exist in a 2D steady flow (where is the liquid entering the cavity via the re-entrant jet going?), it is for that reason not abandoned or rejected by them. They suppose that periods of development of the re-entrant jet, filling the cavity, are followed by periods of emptying. This would imply an intermittent presence of the re-entrant jet. We can hardly imagine such events to happen in the more or less steady flow regime that we study in this paper.

But there is more wrong with Fig. 10. It suggests that the streamline touching the foil at the reattachment point comes from the free stream outside the cavity. Consequently the pressure at the reattachment point should be expected to be close to  $C_p=1.0$ , which not even nearly happens. We think therefore that Fig. 10 is so much in conflict with physical principles and with measured and computed pressures in the stagnation point that it is untenable.

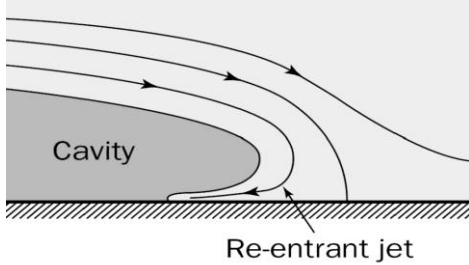


**Figure 10:** Re-entrant jet model in [1]

In the more or less steady regime studied in this paper, the flow behavior can hardly be interpreted as a re-entrant jet flow, let alone an intermittent re-entrant jet flow. Unsteadiness will rather arise from slight fluctuations of the source term. When listing the properties of the source term, we have pointed out that in a steady flow any source in a material volume must be compensated by an equivalent sink (see Eq. (6)). Whenever a slight imbalance occurs, however, the cavity will grow or shrink. So we see then a slight wandering of notably the tail of the cavity, but with a recirculation zone under the tail permanently present.

### Is the cavity a material surface?

From all previous considerations it appears that the liquid-vapour interface is not a material surface, neither at the front end, nor at the aft end of the cavity. As a matter of fact, even where the cavity surface is practically aligned with a streamline some evaporation or condensation may still take place. This becomes clear if we study the distribution of the source term.

Fig. 11 shows two plots of the source term distribution at  $\sigma=1.60$ , one with the  $p=p_v$  isoline and one with the  $\alpha_v=0.5$  contour line included. There is a high peak at the front end of the cavity while the negative sources are all concentrated at the aft end, but less peaky. Evidently, the positive values of the source term are found inside, the negative values outside the  $p=p_v$  contour line. And we verified that in the converged solution the sum of sources and sinks vanishes. Notice further that the cavity contour does not coincide with the  $p=p_v$  isoline.

Clearly the flow field is not source-free. Eq. (6) does not exclude that possibility, however. But is it imaginable that there are no sources or sinks in a flow with a steady cavity? The only possibility would be that the liquid-vapour interface is a material surface throughout. Eq. (7) tells that such condition implies a zero source strength. But even the model illustrated in Fig. 10 is not compatible with that assumption. It would imply that the cavity is bordered by a closed streamline inside a flow recirculation zone (the cavity could fill this zone completely or partially). But why would the flow detach and reattach in those circumstances?

If the vapour-liquid interface is not a material surface, there must be mass and momentum transfer across the interface. Considering the high density difference between liquid (about  $998 \text{ kg/m}^3$  at  $24 \text{ }^\circ\text{C}$ ) and vapour ( $\approx 0.023 \text{ kg/m}^3$  at  $24 \text{ }^\circ\text{C}$ ), such transfers can only take place at low rates to avoid enormous changes in the velocity field. At the front end therefore we see the streamlines entering the vapour region at a very small angle relative to the interface. So the velocity normal to the interface is very small, but finite. At the same time the streamlines diverge strongly. Together they prevent an enormous acceleration of the fluid.

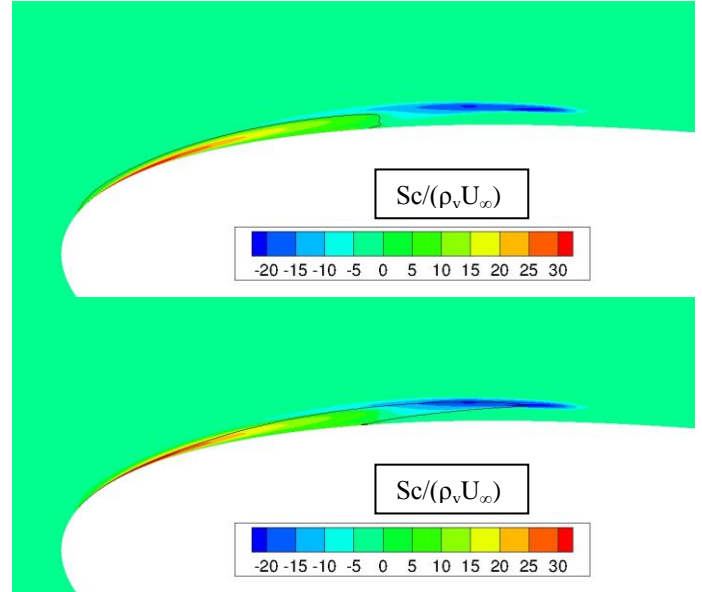


**Figure 11:** Source term distribution at  $\sigma=1.60$  (grid G3) with  $p=p_v$  contour (top) and  $\alpha_v=0.5$  contour (bottom)

The condition of a small angle between streamline and interface cannot be met everywhere at the rear end of the cavity, where locally streamlines leave the vapour region in a direction perpendicular to the interface. In order to reach a gradual mass and momentum transfer the interface is there relatively thick, possibly indicating a break-up of the sheet into bubbles. Also streamline contraction helps to keep the velocity field smooth in the phase transition there.

One might argue that the present numerical approach cannot produce sharp liquid-vapour interfaces and is therefore prone to give misleading results. But imagine that the interface is perfectly sharp while it is not a material surface. Mass conservation then requires that the velocity component normal to the interface increases by a factor  $\rho_l/\rho_v$ , i.e. roughly 40000, across the interface. If that normal velocity would be only 0.025% of the total velocity it would have to jump to 10 times the total velocity. Momentum conservation would require a pressure jump and a continuous tangential velocity component across the interface. So the consequence is an abrupt change of velocity, flow direction and pressure. This seems absurd and it is unlikely that we can have a sharp interface which is not a material surface. There remains the option of a sharp interface which is a material surface. That can occur locally, but not for the entire interface, as we have explained above.

## Overall flow interpretation

Thus we come to the following overall picture of what happens in and around a partial cavity, from the inception phase until the start of vapour shedding. If the pressure drops below the saturated vapour pressure the source term is activated, which results in vapour production. This source term is accompanied by a sink further downstream to establish the phase transition back to liquid (condensation). Flow reversal does not appear at this very early stage close to inception; there is no flow recirculation zone yet. The cavity has a fixed position relative to the foil but the vapour in it is travelling. Remarkable is that the cavity at its rear end is already lifted from the foil surface, so there is liquid beneath the cavity tail in absence of any re-entrant jet or reversed flow.

Flow reversal sets in if the cavitation number is further lowered. It occurs first at the aft end of the cavity, under its tail. The recirculation zone is then completely liquid-filled. But with decreasing cavitation number the flow detachment point moves a little towards the front end of the cavity, while the reattachment point moves downstream with the growth of the length of the cavity; the recirculation zone is then partly filled with vapour, implying a continuous cycle of evaporation and condensation inside that zone. The streamline ending in the reattachment point is evidently not coming from the free stream; it is the streamline bordering the recirculating flow zone. It explains why the pressure at the reattachment point is always far below the stagnation pressure  $C_p=1.0$ .

As an illustration of the global flow pattern, cavity shape and streamlines at  $\sigma=1.4$  are given in a schematic height-scaled plot in Fig. 12. Notice that the dividing streamline, i.e. the streamline bordering the flow recirculation zone, is somewhere in the middle of the cavity until it leaves the cavity at its tail. Notice also the streamline divergence at the front end of the cavity and the streamline convergence in the tail region due to phase changes. The contrast with Fig. 10 is evident.

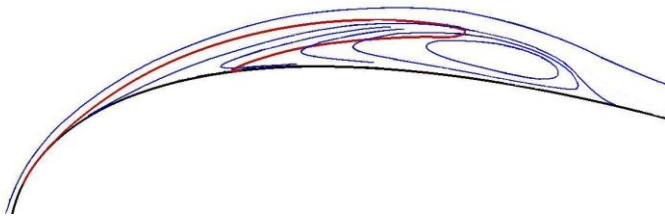


**Figure 12:** Streamline pattern near the cavity (red line) at  $\sigma=1.4$  (height magnified by a factor 2)

Upon lowering  $\sigma$ , the cavity grows in length and height with a strong reduction of the aspect ratio. The conditions at the front end stabilize: the magnitude of the source strength and the difference between minimum and vapour pressure stay almost the same. In the tail region, however, the flow tends to become more and more unstable resulting in unsteady behavior, ultimately leading to shedding of cavitation.

## RELATION WITH EXPERIMENTAL RESULTS

Having described the numerical results in detail, we must now consider how they correlate with experimental data and observations of partial cavities.

In a global sense, i.e. with respect to lift and drag characteristics and cavity length, our results conform well with experimental information. As an example the cavity length predictions are compared with experimental data by Arndt, extracted from [12], in Fig. 13. The cavity length is plotted versus  $\sigma/2\alpha$ , where  $\alpha$  is the angle of attack in radians. Although the computations relate to small cavities only, they fit nicely with the experimental data covering a wider range.

But the main interest here is in the details of the flow in and near the cavity. In that respect, Arakeri and Acosta [13, 14] were the first to demonstrate, by using the schlieren technique in a water tunnel experiment, the strong relation between cavitation and the behaviour of the boundary layer. A remarkable set of papers on the same subject was subsequently produced at the University of Grenoble by the group of Franc and Michel [15, 16, 17, 18]. Further corroboration of results came from Ceccio and co-workers in Michigan [19, 20], and many others [e.g. 21, 22, 23].

The global picture that has evolved from these studies is that if the wetted flow shows laminar boundary layer separation followed by reattachment due to transition to a turbulent flow condition, cavitation inception and development occurs inside the separation bubble. If there is no laminar separation, there either appears no cavitation at all (liquid under tension) or cavitation appears as isolated traveling bubbles, the bubble density varying strongly with the nuclei spectrum of the inflow and other details of the experimental set-up. The bubble density may be high enough to produce narrow banded or wedge-shaped attached cavities, dependent on liquid and foil surface properties.

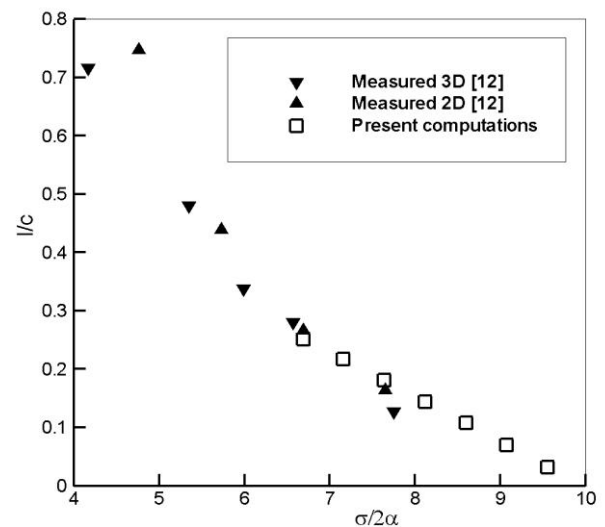


**Figure 13:** Computed cavity length compared with experimental data

We recall that for the case studied in this paper, the wetted flow is free of boundary layer separation. Which means that

flow conditions differ from those of most of the above cited experiments. But one thing is clear: our numerical cavitation model can in its present form not simulate traveling bubble cavitation. It says that evaporation starts, possibly at a slow rate but anyway, at any location where at a given instant the pressure is below the vapour pressure. The role of the parameter  $n_0$ , the “number of nuclei per unit of volume”, is only to change the strength of the source term. We would have to add stochastic properties to let the evaporation start dependent on the availability of a nucleus for instance. Consequently, as we have observed above, at the early stages of computed cavity development, the computed cavity is seemingly attached, having the appearance of a sheet, but the vapour is traveling. This is in accordance with at least the experiments of Zhang *et al.* [21], further analysed in [22]. They report that just after inception there is no reverse flow anywhere around the closure region of the cavitation. The cavity simply closes, while the velocity component parallel to the foil surface remains positive. It is also consistent with a study by Farhat *et al.* [23]. They report that “*exploding nuclei continuously feed the attached cavity at its detachment location, travel inside the cavity and collapse as they escape at the cavity closure*”. That laminar separation of the boundary layer is not required for the development of an attached cavity has thus been shown in some experiments and is corroborated by our numerical simulations.

But our numerical results further show that flow separation is invoked pretty soon after inception. Already for  $\sigma=1.90$  the flow under the tail stagnates, while inception is at  $\sigma=2.08$ . So it is not surprising that in many experiments partial cavitation and boundary layer separation go hand in hand.

But conspicuously experimentalists systematically report flow separation to occur upstream of the cavity, while that in our numerical simulations never happens. Experimentalists admit that in their flow concept there must be a region upstream of the cavity where the pressure is below vapour pressure without causing cavitation (the ‘cavity detachment paradox’ [19]). Thus the existence of a small region at the front end of the cavity where the pressure is below the vapour pressure was conjectured [1, 5] and later also measured [19, 23]. Interesting is that our numerical results clearly support at least this aspect of the problem and even indicate that it is a necessary condition. But in the numerical solutions vapour production starts in this region and cavitation appears before flow reversal sets in.

We can only speculate about the reason for this apparent discrepancy between measurements and computations. One such speculation is that the strong streamline divergence at the front end of the cavity has wrongly been interpreted by experimentalists as flow detachment. Particularly when he/she is biased to think of a cavity surface as a material surface such interpretation could easily be made. Consider for example the flow pattern at the top of Fig. 6. If only the streamlines outside the cavity were available, it would seem that the flow is separating where the cavity starts, while actually it does so only much further downstream.

Another concern is the possibility of scale effects and the nuclei content of the inflow. We observed that most of the above-cited experimental work has been done on small test

objects. For small objects the onset flow speed must be high to obtain a sufficiently high Reynolds number, so that the time scale  $c/U_\infty$  is small. Since nuclei need a finite time to grow to visible cavitation this time scale may be relevant. With regard to nuclei one might also say that in the computations suitable nuclei are unconditionally available at any location where the pressure drops below the vapour pressure. In an experiment this may not be so and evaporation may not occur or be delayed, while in the computations only the evaporation rate is variable.

Evidently, here is a topic for discussion and also maybe a challenge for further experiments, e.g. to measure the flow inside the cavity.

## CONCLUSIONS

Assuming a fluid of variable density, we have made numerical simulations of the partial cavity on a 2D NACA0015 foil in the early stages of its development. The RANS equations supplemented with a turbulence model and a cavitation model form the mathematical model. Some effort has been made to explain the main features and the consequences of employing a model of this kind. By using three geometrically similar grids we could get an impression of grid density effects on the solution.

The results have shown that just after inception a very thin attached cavity appears in which vapour is created at the front end, which travels with the flow and condensates at the rear end. The implication is that the liquid-vapour interface is not a material surface. Upon lowering the cavitation number the cavity grows and a flow recirculation zone appears under the tail of the cavity. By further lowering the cavitation number the flow detachment point moves a little towards the location of minimum pressure on the suction side of the foil but stays downstream of the front end of the cavity, while the reattachment point moves aft with the tail of the cavity. Initially the flow recirculation zone is completely liquid-filled, but for lower cavitation numbers it contains vapour as well, so that it is partly overlapping with the cavity. Although the flow recirculation zone implies near-wall flow in the direction opposite to the main flow one can hardly call it a re-entrant jet.

Some important conclusions are:

- We were able to explain why the pressure at flow reattachment is far below the stagnation pressure.
- We have confirmed experimental evidence that the liquid just ahead of the cavity is under tension.
- We have made plausible that the liquid-vapour interface cannot be a material surface.
- We have given evidence that an attached cavity is not necessarily associated with flow detachment.

As a corollary the re-entrant jet model suggested by free streamline theory as a model for the cavity closure must be considered as invalid for more or less steady partial cavities.

We do not claim that our numerical results represent the truth. Also we have no doubt that the numerical models for cavitation need to be extended and improved to cover a wider range of experimentally observed phenomena. But the mathematical model used has a sound physical basis. We are therefore confident enough to conjecture that the flow behavior in and near a partial cavity is quite different from what has been assumed for a long time. It is now up to other numerical

analysts, but certainly to experimentalists as well, to corroborate or to falsify the flow picture evolving from our results.

## ACKNOWLEDGMENTS

Part of this work has been carried out under the Sixth Framework European Project VIRTUE.

## NOMENCLATURE

$c$	chord length
$CD$	non-dimensional drag force per unit span
$CL$	non-dimensional lift force per unit span
$Cp$	$= (p - p_\infty) / (1/2 \rho U_\infty^2)$
$\ell$	cavity length (measured on $\alpha_v = 0.5$ contour)
$\vec{u}$	velocity vector
$U_\infty$	undisturbed inflow (=reference) speed
$p$	pressure
$p_v$	saturated vapour pressure
$p_\infty$	outlet (=reference) pressure
$Rn$	Reynolds number
$S$	source function in $\alpha_v$ -equation
$\alpha_v$	vapour volume fraction
$\rho$	mass density of mixture fluid
$\sigma$	$= (p_\infty - p_v) / (1/2 \rho U_\infty^2)$

Subscripts:

$l$	liquid
$v$	vapour

## REFERENCES

- [1] Franc, J.-P. and Michel, J.-M. 2004, *Fundamentals of Cavitation*, Kluwer Academic Publishers, Dordrecht, The Netherlands.
- [2] Batchelor, G. K. 1967, *An Introduction to Fluid Dynamics*, Cambridge University Press, London.
- [3] Menter, F. R. 1994, "Two-equation eddy-viscosity turbulence models for engineering applications", *AIAA Journal*, 32, 1598-1605.
- [4] Sauer, J. 2000, "Instationär Kavitierende Strömungen – Ein neues Modell, basierend auf Front-Capturing (VoF) und Blasendynamik", PhD Thesis, University of Karlsruhe, Germany.
- [5] Franc, J.-P. et al. 1995, *La Cavitation, Mécanismes Physiques et Aspects Industriels*, Presses Universitaires de Grenoble, France.
- [6] Kunz, R.F., Boger, D.A., Stinebring, D.R., Chyczewski, T.S., Gibeling, H.J. and Govindan, T.R. 1999, "Multi-phase CFD analysis of natural and ventilated cavitation about submerged bodies", Proc. of 3<sup>rd</sup> ASME/JSME Joint Fluids Engineering Conference, San Francisco, California (FEDSM'99-7364).
- [7] Hoekstra, M., Vaz, G., Abeil, B. and Bunnik, T. 2007, "Free-surface modeling with interface capturing techniques", MARINE2007 Conf., Barcelona, Spain.
- [8] Vaz, G., Jaouen, F. and Hoekstra, M., 2009, "Free-surface viscous flow computations. Validation of URANS code FreSCo", Proc. ASME 28<sup>th</sup> Int. Conf. on Ocean, Offshore and Arctic Engineering OMAE2009, Honolulu, HAWAII.
- [9] Abbott, I. A. and von Doenhoff, A. E., 1958, *Theory of Wing Sections*, Dover Publications, New York 19
- [10] Ahuja, V., Hosangadi, A. and Arunajatesan, S. 2001, "Simulations of cavitating flows using hybrid unstructured meshes", *J. Fluids Engineering*, Vol. 123, pp. 331-340.
- [11] Leroyer, A. 2004, "Étude du couplage écoulement/movement pour des corps solides ou à déformation impose par resolution des equations de Navier-Stokes. Contribution à la modélisation numérique de la cavitation", PhD Thesis, École Centrale de Nantes, France.
- [12] Berntsen, G.S., Kjeldsen, M. and Arndt, R.E.A.. 2001, "Numerical modeling of sheet and tip vortex cavitation with Fluent 5", Proc. of CAV2001, California Institute of Technology, Pasadena, California, USA.
- [13] Arakeri, V.H. 1975, "Viscous effects on the position of cavitation separation from smooth bodies", *J. Fluid Mech.*, Vol. 68, part 4, pp. 779-799.
- [14] Arakeri, V.H. and Acosta, A.J. 1976, "Cavitation inception observations on axisymmetric bodies at supercritical Reynolds numbers", *J. Ship Research*, Vol. 20, No. 1, pp. 40-50.
- [15] Franc, J.-P. and Michel, J.-M. 1985, "Attached cavitation and the boundary layer: experimental investigation and numerical treatment", *J. Fluid Mech.*, Vol. 154, pp. 63-90.
- [16] Franc, J.-P. and Michel, J.-M. 1988, "Unsteady attached cavitation on an oscillating hydrofoil", *J. Fluid Mech.*, Vol. 193, pp. 171-189.
- [17] Brianchon-Marjollet, L., Franc, J.-P. and Michel, J.-M. 1990, "Transient bubbles interacting with an attached cavity and the boundary layer", *J. Fluid Mech.*, Vol. 218, pp. 355-376.
- [18] Callenaere, M., Franc, J.-P., Michel, J.-M., and Riondet, M. 2001, "The cavitation instability induced by the development of a re-entrant jet", *J. Fluid Mech.*, Vol. 444, pp. 223-256.
- [19] Tassin Leger, A. and Ceccio, S.L. 1998, "Examination of the flow near the leading edge of attached cavitation. Part 1: detachment of two-dimensional and axisymmetric cavities", *J. Fluid Mech.*, Vol. 376, pp. 61-90.
- [20] Labertaux, K.R. and Ceccio, S.L. 2001, "Partial cavity flows. Part 1: Cavities forming on models without spanwise variation", *J. Fluid Mech.*, Vol. 431, pp. 1-41.
- [21] Zhang, Y., Gopalan, S. and Katz, J. 1998, "On the flow structure and turbulence in the closure region of attached cavitation", Proc. 22<sup>nd</sup> Symposium on Naval Hydrodynamics, Washington D.C.
- [22] Gopalan, S. and Katz, J. 2000, "Flow structure and modeling issues in the closure region of attached cavitation", *Physics of Fluids*, Vol. 12, No. 4, pp. 895-911.
- [23] Farhat, M., Guennoun, F. and Avellan, F. 2002, "The leading edge cavitation dynamics", Proc. of ASME 2002 Fluids Engineering Division Summer Meeting, Montreal, Quebec, Canada (FEDSM'02-31000).